# Equilibrium and stability in a heliotron with anisotropic hot particle slowing-down distribution

W. A. Cooper, Y. Asahi, Y. Narushima, Y. Suzuki, K. Y. Watanabe et al.

## Related Articles

Perpendicular and tangential angularly resolved multi-sight neutral particle analyzer system in LHD
Rev. Sci. Instrum. 83, 10D920 (2012)

Diagnostics development for quasi-steady-state operation of the Wendelstein 7-X stellarator (invited)
Rev. Sci. Instrum. 83, 10D730 (2012)

Effect of superbanana diffusion on fusion reactivity in stellarators
Phys. Plasmas 19, 082516 (2012)

The internal disruption as hard Magnetohydrodynamic limit of 1/2 sawtooth like activity in large helical device
Phys. Plasmas 19, 082512 (2012)

Internal disruptions and sawtooth like activity in Large Helical Device
Phys. Plasmas 19, 082501 (2012)
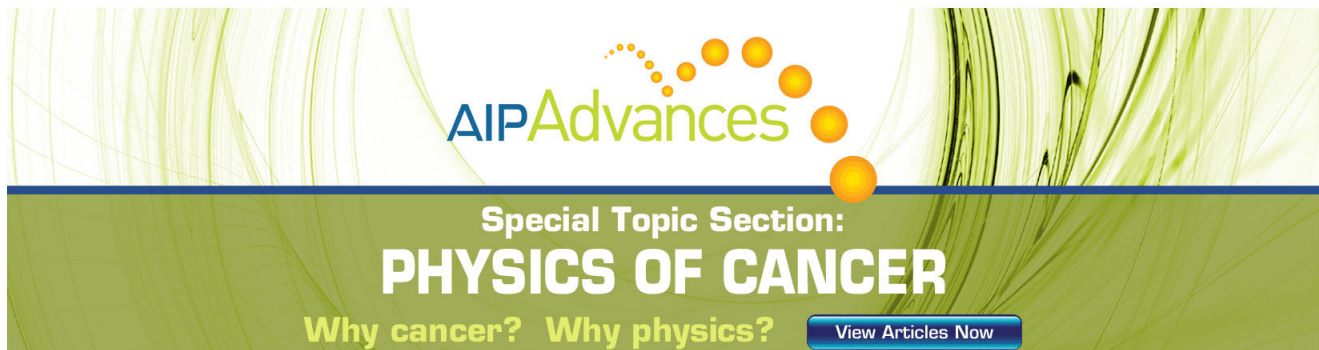
## Additional information on Phys. Plasmas

Journal Homepage: http://pop.aip.org/

Journal Information: http://pop.aip.org/about/about_the_journal

Top downloads: http://pop.aip.org/features/most_downloaded

Information for Authors: http://pop.aip.org/authors

# Equilibrium and stability in a heliotron with anisotropic hot particle slowing-down distribution

W. A. Cooper,[1,2,a)] Y. Asahi,[2] Y. Narushima,[2] Y. Suzuki,[2] K. Y. Watanabe,[2] J. P. Graves,[1] and M. Yu. Isaev[3]

[1]*Ecole Polytechnique Fédérale de Lausanne (EPFL), Centre de Recherches en Physique des Plasmas, Association Euratom-Confédération Suisse, CH1015 Lausanne, Switzerland*
[2]*National Institute for Fusion Science, Oroshi-cho, 322-6, Toki-shi 509-5292, Japan*
[3]*Russian Research Centre "Kurchatov Institute," 123182 Moscow, Russia*

The equilibrium and linear fluid Magnetohydrodynamic (MHD) stability in an inward-shifted large helical device heliotron configuration are investigated with the 3D ANIMEC and TERPSICHORE codes, respectively. A modified slowing-down distribution function is invoked to study anisotropic pressure conditions. An appropriate choice of coefficients and exponents allows the simulation of neutral beam injection in which the angle of injection is varied from parallel to perpendicular. The fluid stability analysis concentrates on the application of the Johnson-Kulsrud-Weimer energy principle. The growth rates are maximum at $\langle \beta \rangle \sim 2\%$, decrease significantly at $\langle \beta \rangle \sim 4.5\%$, do not vary significantly with variations of the injection angle and are similar to those predicted with a bi-Maxwellian hot particle distribution function model. Stability is predicted at $\langle \beta \rangle \sim 2.5\%$ with a sufficiently peaked energetic particle pressure profile. Electrostatic potential forms from the MHD instability necessary for guiding centre orbit following are calculated.
[http://dx.doi.org/10.1063/1.4757635]

## I. INTRODUCTION

The principal methods to heat ions in stellarator magnetic confinement systems involve the application of either neutral beam injection (NBI) or ion cyclotron heating (ICRH). The large helical device (LHD) has both types of heating mechanisms,[1] but most of the input power relies on 10 MW tangential NBI system with 180 keV per beam ion. The volume averaged $\langle \beta \rangle$ achieved exceeds 4%.[2] The ratio of stored energy in the parallel direction (to the magnetic field lines) compared with the perpendicular direction can reach a level of 4 at low plasma density $(1 \times 10^{19} \text{m}^{-3})$.[3]

Magnetohydrodynamic (MHD) equilibrium solvers for isotropic pressure plasmas are very common, but anisotropic pressure models have not been widely explored. Nevertheless, four axisymmetric tokamak equilibrium codes have been previously developed,[4–7] as well as another for helically symmetric stellarators.[8] For general three-dimensional (3D) magnetic confinement configurations, analytic developments[9,10] have contributed to foster extensions of the 3D VMEC code[11] with imposed nested magnetic flux surfaces under fixed[12] and free[13] boundary conditions using a modified slowing-down beam particle distribution function for perpendicular[14] and parallel[15] injection in which fixed boundary applications were investigated. Subsequently, a bi-Maxwellian particle distribution function model was considered and implemented in the VMEC code.[16] The free boundary extension, named ANIMEC, has employed the bi-Maxwellian form and was applied to a two-field period quasiaxisymmetric stellarator.[17] In this work, we shall explore a combination of the slowing-down distributions treated in Refs. 14 and 15 and demonstrate that

we can model neutral beam injection angles that span the range from the direction parallel to that perpendicular with respect to the magnetic field lines. This model is implemented as an option in the ANIMEC code.

There are currently three linear MHD stability codes adapted to 3D magnetic confinement configurations. The ideal code CAS3D,[18] the extended ideal code TERPSICHORE[19,20] that includes anisotropic pressure models[16,21] and the resistive SPECTOR3D code.[22] Two fluid anisotropic pressure MHD stability models have been implemented in the 3D TERPSICHORE code. The energy principle derived by Kruskal and Oberman (KO)[23] retains the full interaction of pressure gradients and current density in the instability drive mechanisms. An alternative energy principle proposed by Johnson, Kulsrud, and Weimer (JKW)[24] considers the hot particle pressure gradients and current density associated with the fast species to be weakly interacting. This model may have very useful applications for modeling the LHD experiment.[2] We examine the fluid MHD stability of the anisotropic pressure equilibria generated with the slowing-down distribution function pressure moments modules implemented in the ANIMEC code, concentrating mostly on the predictions of the JKW stability model in an inward-shifted LHD heliotron configuration. The kinetic energy in the TERPSICHORE code has been extended to allow for a more physical kinetic energy normalisation.

In Sec. II, we briefly describe the 3D MHD equilibrium approach used in the ANIMEC code. In Sec. III, we present the slowing-down distribution function model we invoke for balanced neutral beam injection simulations. In Sec. IV, applications to the LHD heliotron with the ANIMEC code are outlined. The linear fluid MHD stability description and the kinetic energy normalisation developed are considered in

a)e-mail: wilfred.cooper@epfl.ch.

Sec. V. The stability computations of the anisotropic equilibrium states obtained with ANIMEC in Sec. IV are investigated in Sec. VI. Two different models for the determination of the electrostatic potential associated with MHD instabilities are compared in Sec. VII. Summary and conclusions are discussed in Sec. VIII.

## II. 3D MAGNETOHYDRODYNAMIC EQUILIBRIA

MHD equilibrium states with nested magnetic flux surfaces and anisotropic pressure are computed with the ANIMEC code,[17] and extended version of the VMEC code.[11–13] This formulation minimises the total energy

$$\mu_0 W = \iiint d^3 x \left[ \frac{B^2}{2} + \frac{\mu_0 p_{\|}(s,B)}{\Gamma - 1} \right], \quad (1)$$

where $B$ is the magnetic field strength, $\mu_0$ is the permeability of free space ($\mu_0 = 4\pi \times 10^{-7} \text{H/m}$), the total pressure parallel to the magnetic field is

$$p_{\|}(s,B) = \mathcal{M}(s)[\Phi'(s)]^{\Gamma} \frac{1 + p_h(s)H(s,B)}{\langle 1 + p_h(s)H(s,B)\rangle^{\Gamma}}, \quad (2)$$

with $\mathcal{M}(s)$ the plasma mass, and $\Phi(s)$ the toroidal magnetic flux function. The radial variable $s$ ($0 \leq s \leq 1$) is proportional to $\Phi$. The amplitude factor $p_h(s)$ controls the hot particle contribution to the parallel pressure, $H(s,B)$ describes the variation of the pressure around a magnetic flux surface, $\Gamma$ is the adiabatic index, $\langle A \rangle$ identifies the flux surface average of $A$, and the symbol prime ($'$) denotes a derivative with respect to the $s$. A steepest descent energy minimisation procedure is applied to generate the equilibrium state coupled with a Fourier decomposition in the poloidal and toroidal angular variables. A preconditioner suppresses the residual force errors down to machine level precision. Invoking Ampere's law, the current density is expressed as $\mu_0 K = \nabla \times (\sigma B)$, where $\sigma = 1 - \mu_0(p_{\|} - p_{\perp})/B^2$ corresponds to the firehose stability parameter.[9]

## III. A MODIFIED SLOWING-DOWN FAST ION DISTRIBUTION FUNCTION

We attempt to determine the fast particle contribution to the pressures by evaluating the corresponding moments of a distribution function. Typically, a bi-Maxwellian distribution function for the energetic species has formed the foundation of fixed and free boundary equilibrium investigations in the past.[16,17] This form was particularly useful and relevant for ICRH simulations. Alternatively, a modified slowing-down distribution given by

$$F_h(s, \mathcal{E}, \lambda) = \frac{1}{2\pi} \frac{I_h \tau_s S(s)}{v^3 + v_c^3} [\lambda B_m(s)]^N, \quad (3)$$

has been proposed and evaluated for perpendicular pressure anisotropy.[14] The amplitude that multiplies the term in brackets constitutes the standard slowing-down distribution function,[25] where $I_h$ is the fast particle beam current, $\tau_s$ is the slowing-down time, $S$ is the source profile, $v$, $\mathcal{E}$, and $\lambda$ are the

particle velocity, energy, and pitch angle, respectively. $B_m$ is usually the minimum value of $B$ on a flux surface and $v_c$ is defined as the critical velocity.[25] Subsequently, a similar model for balanced tangential beam injection was examined,[15] where the distribution function was expressed as

$$F_h(s, \mathcal{E}, \lambda) = \frac{1}{2\pi} \frac{I_h \tau_s S(s)}{v^3 + v_c^3} [1 - \lambda B_m(s)]^L. \quad (4)$$

We propose in this work a combination of the forms described by Eqs. (3) and (4), which allows the modeling of balanced neutral beam injection. Different angles of injection can be simulated with the appropriate addition and subtraction of terms with different exponents $L$ and $N$. In particular, we write

$$F_h(s, \mathcal{E}, \lambda) = \frac{1/2\pi}{\sum_0^L a_\ell^{\|} + \sum_0^N a_n^{\perp}} \frac{I_h \tau_s S(s)}{v^3 + v_c^3}$$
$$\times \left[ \sum_{\ell=0}^L \frac{a_\ell^{\|}}{\sum_0^\ell f_k} [1 - \lambda B_m(s)]^\ell + \sum_{n=0}^N \frac{a_n^{\perp}}{q_n} [\lambda B_m(s)]^n \right], \quad (5)$$

where $a_\ell^{\|}$ ($a_n^{\perp}$) correspond to coefficients associated with the injection of beam ions parallel (perpendicular) to the equilibrium field lines. We define

$$q_n \equiv \frac{3 \times 2^n n!}{[2(n+1)+1]!!}$$

$$f_k \equiv \frac{3 \times (-2)^k \ell!}{[2(k+1)+1]!!(\ell - k)!}.$$

The calculations undertaken in this paper concentrate on three specific cases. The choices $a_0^{\|} = 0.01$, $a_7^{\|} = 1$ $a_8^{\|} = -0.88$ yield the distribution function in the $v_{\perp}$ versus $v_{\|}$ space in Fig. 1, which corresponds to an injection angle $\theta_b \sim 18°$ with respect to the direction of the $B$-lines. The remaining coefficients $a_j^{\|} = 0$, $a_j^{\perp} = 0$. For an injection angle $\theta_b \sim 43.5°$, the following choice is required: $a_0^{\|} = 0.08$, $a_1^{\|} = 1$, and $a_2^{\|} = -0.7$ (the remaining coefficients vanish). This is shown in Fig. 2. Finally, for a more nearly perpendicular injection angle, we chose $a_0^{\perp} = 0.1$, $a_4^{\perp} = 1$, and $a_5^{\perp} = -0.75$, which yields an injection angle $\theta_b \sim 68°$ with respect to the direction of $B$, as pictured in Fig. 3.

The parallel pressure is given by the equation $p_{\|}(s,B) = p_{th}(s)[1 + p_h(s)H(s,B)]$, where the shaping factor of the hot particle pressure around the flux surfaces is
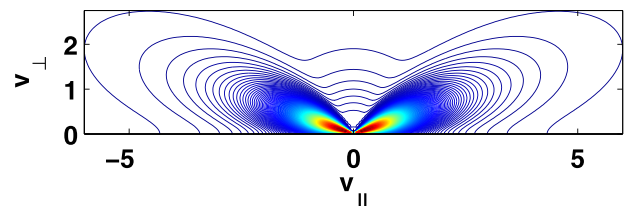


FIG. 1. Hot particle distribution function obtained with coefficients $a_0^{\|} = 0.01$, $a_7^{\|} = 1$, and $a_8^{\|} = -0.88$ in the $v_{\perp}$ versus $v_{\|}$ space. All other coefficients $a_j^{\|} = 0$, $a_j^{\perp} = 0$. The function is evaluated at $B = B_m$. The beam injection angle is $\theta_b \sim 18°$.

FIG. 2. Hot particle distribution function obtained with coefficients $a_0^{\|} = 0.08$, $a_1^{\|} = 1$, and $a_2^{\|} = -0.7$ in the $v_\perp$ versus $v_\|$ space. All other coefficients $a_j^\perp = 0$, $a_j^{\|} = 0$. The function is evaluated at $B = B_m$. The beam injection angle is $\theta_b \sim 43.5°$.

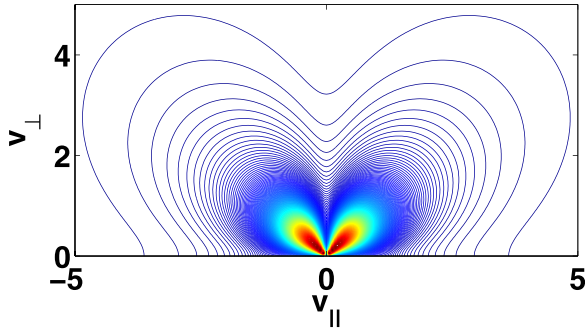$$H(s,B) = \frac{1}{\sum_0^L a_\ell^{\|} + \sum_0^N a_n^\perp} \left\{ \sum_{\ell=0}^{L} \frac{a_\ell^{\|}}{\sum_0^\ell f_k} \sum_{k=0}^{\ell} \left[ \frac{B_m(s)}{B} \right]^k \right.$$
$$\left. + \sum_{n=0}^{N} a_n^\perp \left[ \frac{B_m(s)}{B} \right]^n \right\}.$$

(6)

For the computation of equilibria, we must prescribe the plasma mass $\mathcal{M}(s)$ (which corresponds directly to the thermal pressure $p_{th}(s)$ when $\Gamma = 0$), the hot particle pressure profiles is controlled with input values to $p_h(s)$, and the toroidal current profile (or the rotational transform). The pressure anisotropy due to the energetic particle species is varied with choices for the exponents $L$ and $N$ and the coefficients $a_\ell^{\|}$ and $a_n^\perp$. Once $p_\|(s,B)$ is determined, parallel force balance is invoked to obtain $p_\perp(s,B)$ and consequently the firehose stability criterion parameter $\sigma$.[9] For diagnostic purposes, we have to calculate $\sqrt{g}\partial p_\|/\partial s|_B$ and the mirror stability criterion parameter $1 + (\mu_0/B)\partial p_\perp/\partial s|_B$.[9] Finally, for MHD stability analysis, we derive also $\sqrt{g}\partial p_\perp/\partial s|_B$.
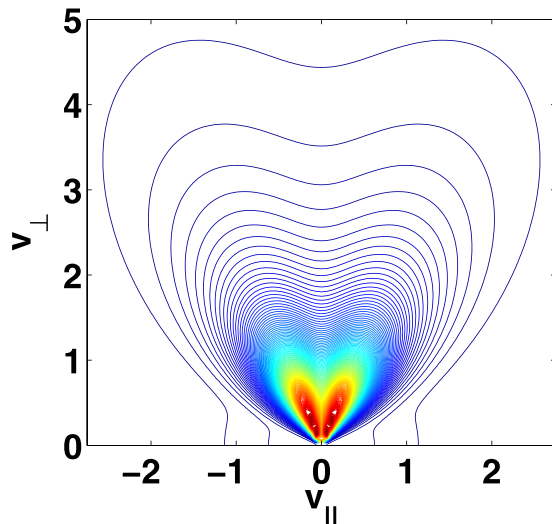


FIG. 3. Hot particle distribution function obtained with coefficients $a_0^\perp = 0.1$, $a_4^\perp = 1$, and $a_5^\perp = -0.75$ in the $v_\perp$ versus $v_\|$ space. All other coefficients $a_j^\perp = 0$, $a_j^{\|} = 0$. The function is evaluated at $B = B_m$. The beam injection angle is $\theta_b \sim 68°$.

## IV. EQUILIBRIUM COMPUTATIONS IN A 10-FIELD PERIOD HELIOTRON

The 3D ANIMEC equilibrium code, which has been adapted to include the anisotropic pressure model described in Sec. III, is employed to compute MHD equilibrium states in a 10 field period heliotron configuration to simulate the LHD device. We specifically select a strongly inward-shifted configuration in which the magnetic axis is located at $R_{ax} = 3.55$ m in the vacuum state. As this configuration does not have a vacuum magnetic well, it is susceptible to MHD instabilities even at very low $\langle \beta \rangle$, which we shall verify in Sec. VI. For simplicity, we choose vanishing net toroidal current within each flux surface, namely $2\pi J(s) = 0$. With $\Gamma = 0$, the thermal pressure is prescribed as $p(s) = p_{th}(s) = p(0)(1-s)(1-s^4)$. This is close to the measured profiles extracted from experimental observations in LHD. For most of the calculations in this paper, the hot particle pressure factor $p_h(s)$ is prescribed as $0.5(1-s) + 0.5(1-s)^2$. The thermal pressure profiles and the flux surface averaged hot particle pressure profiles that result from the choices of $p_{th}(s)$ and $p_h(s)$ are summarised in Fig. 4 for the three different anisotropic cases ($\theta_b \sim 18°$, $\theta_b \sim 43.5°$, and $\theta_b \sim 68°$) under consideration at $\langle \beta \rangle = 4.45\%$. Here, we define $\langle \beta \rangle \equiv \int \int \int d^3 x \mu_0(p_\| + p_\perp)/B^2$. The fast particle $\langle \beta^h \rangle \sim \langle \beta \rangle/3$ for all computations presented in this article. The rotational transform profiles for zero toroidal current at $\langle \beta \rangle = 4.45\%$ for the 3 different injection angles are displayed in Fig. 5. They do not vary significantly with respect to changes in $\theta_b$.

## V. LINEAR FLUID MHD STABILITY THEORY

The energy principles with anisotropic that are implemented in the TERPSICHORE code include a fully interactive model proposed by KO[23] and a rigid hot particle model devised by JKW.[24] All of the calculations presented in this article (except for that corresponding to the curve with black
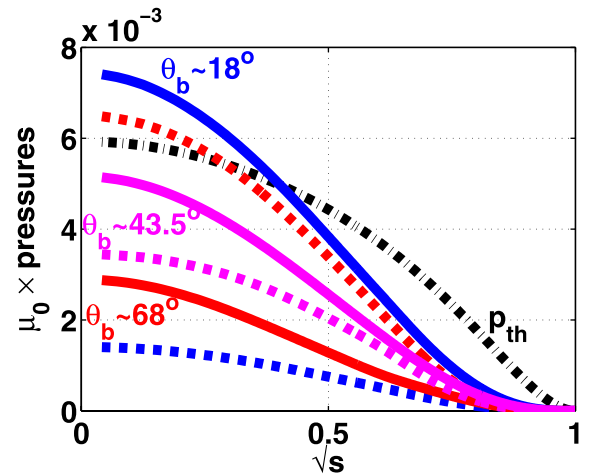


FIG. 4. The pressure profiles as a function of $\sqrt{s}$ for an inward-shifted LHD configuration at $\langle \beta \rangle = 4.45\%$ for injection angles of $\theta_b \sim 18°$, $\theta_b \sim 43.5°$, and $\theta_b \sim 68°$ with respect to the field lines. The solid lines correspond to $\langle p_\|^h \rangle$, the flux surface averaged component of the hot particle parallel pressure, the dashed lines correspond to $\langle p_\perp^h \rangle$, and the flux surface averaged component of the hot particle perpendicular pressure. The broader profile corresponds to the thermal pressure. All pressures are multiplied by $\mu_0$.
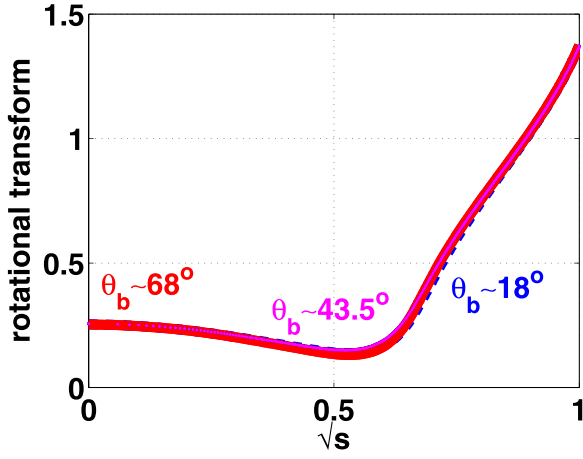
FIG. 5. The rotational transform profiles as a function of $\sqrt{s}$ for an inward-shifted LHD configuration at $\langle\beta\rangle = 4.45\%$ for injection angles of $\theta_b \sim 18°$, $\theta_b \sim 43.5°$, and $\theta_b \sim 68°$ with respect to the field lines. The rotational transform profiles are almost the same regardless of injection angle.

squares in Fig. 8) are based on the JKW energy principle because experimental observations on the LHD device suggest that this energy principle more accurately reflects the measurements.[2] The stability code evaluates

$$\delta W_p + \delta W_V - \omega^2 \delta W_K, \tag{7}$$

where $\delta W_p$ is the internal plasma potential energy, $\delta W_V$ is the vacuum energy, and $-\omega^2 \delta W_K$ represents the kinetic energy. The kinetic energy term $\delta W_K$ is given by

$$\mu_0 \delta W_K = \frac{1}{2} \int_0^{2\pi/L_s} d\phi \int_0^{2\pi} d\theta \int_0^1 ds \sqrt{g} \mu_0 (\boldsymbol{\xi} \cdot \boldsymbol{\rho_M} \cdot \boldsymbol{\xi}), \tag{8}$$

where $L_s$ is the number of equilibrium field periods per stability period, $\theta$ and $\phi$ are the Boozer coordinate poloidal and toroidal angles, respectively, $\boldsymbol{\rho_M}$ is the plasma mass tensor and the displacement vector under the plasma incompressibility assumption is

$$\boldsymbol{\xi} = \sqrt{g}\xi^s \nabla\theta \times \nabla\phi + \frac{\boldsymbol{B} \times \nabla s}{B^2}\eta. \tag{9}$$

Previous applications of the TERPSICHORE code[19] invoked a mass tensor dyadic expressed as

$$\boldsymbol{\rho_M} = \nabla s \nabla s + \frac{[\sqrt{g}\boldsymbol{B} \times (\nabla\theta \times \nabla\phi)][\sqrt{g}\boldsymbol{B} \times (\nabla\theta \times \nabla\phi)]}{[2\Phi'(s)]^2}, \tag{10}$$



FIG. 7. Bi-Maxwellian distribution function with a parallel to perpendicular temperature ratio $T_{||}/T_\perp \sim 5$, which yields an equilibrium state with the same ratio $\langle\beta_{||}^h\rangle/\langle\beta_\perp^h\rangle \sim 5$ as in Fig. 1.

which yields the simplified kinetic energy integrand

$$\mu_0 \boldsymbol{\xi} \cdot \boldsymbol{\rho_M} \cdot \boldsymbol{\xi} = (\xi^s)^2 + \frac{1}{[2\Phi'(s)]^2}\eta^2. \tag{11}$$

A more physical kinetic energy requires the mass tensor to be $\boldsymbol{\rho_M} = \rho_M \boldsymbol{I}$, proportional to the identity tensor. Under these circumstances, the kinetic energy integrand acquires the form

$$\mu_0 \boldsymbol{\xi} \cdot \boldsymbol{\rho_M} \cdot \boldsymbol{\xi} = \mu_0 \rho_M \left[ g_{ss}(\xi^s)^2 - \frac{2}{\sigma\sqrt{g}B^2}[I(s)g_{s\theta} + J(s)g_{s\phi}]\xi^s\eta + \frac{|\nabla s|^2}{B^2}\eta^2 \right], \tag{12}$$

where $g_{ij}$ represents a lower metric element while the poloidal and toroidal current flux functions are $I$ and $J$, respectively. The computations in this work adopt this more physically relevant kinetic energy norm. The fixed and free boundary mode structures and growth rates of a benchmark calculation involving a number of different MHD stability codes[26] have been successfully recovered with this upgraded kinetic energy normalisation.

We investigate free boundary stability of LHD configurations by prescribing a conducting wall far from the plasma of similar shape but much smoother than the vacuum vessel in the device. The specific shape at various cross sections is displayed in Fig. 6.

## VI. LINEAR FLUID MHD STABILITY APPLICATIONS TO LHD

The linear fluid MHD stability of the ANIMEC equilibria described in Sec. IV with respect to the $n = 2$ family of modes[27–29] is investigated with the TERPSICHORE code[19,30] for the inward-shifted LHD configuration. We compare the growth rate of the case with a slowing-down distribution with injection angle $\theta_b \sim 18°$ with that of a bi-Maxwellian distribution, shown in Fig. 7, with the same ratio $\langle\beta_{||}^h\rangle/\langle\beta_\perp^h\rangle \sim 5$. The growth rates are normalised to the
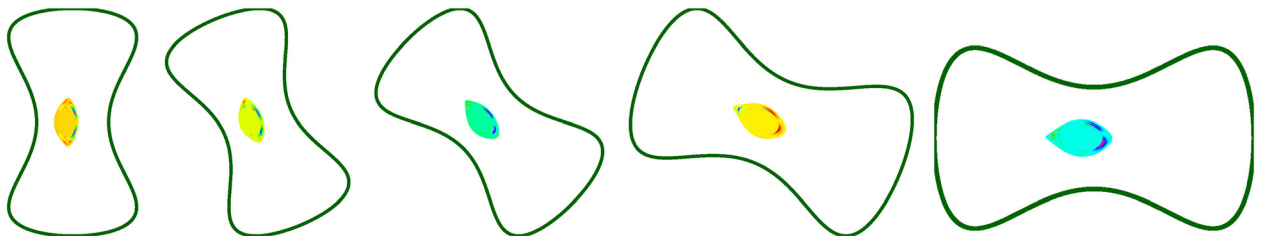


FIG. 6. The conducting wall prescribed for free boundary terpsichore fluid MHD stability simulations that enclose the plasma at five different cross sections spanning half of a field period in an inward-shifted LHD configuration. The perturbed radial magnetic field distribution within the plasma is plotted at each cut.
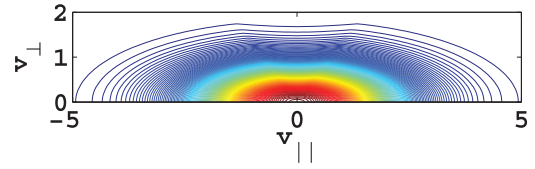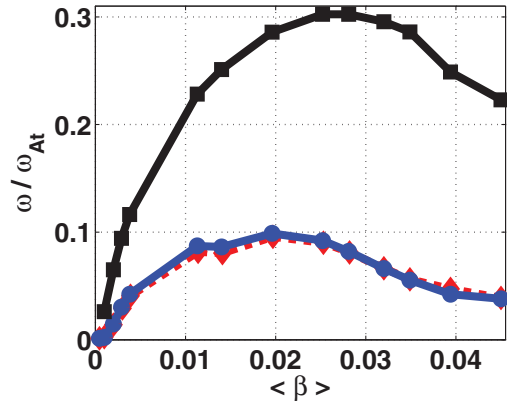
FIG. 8. Growth rate normalised to the toroidal Alfvén frequency for an inward-shifted LHD configuration with nearly parallel beam injection pressures as a function of $\langle \beta \rangle$ from a modified slowing-down distribution function according to the KO energy principle (squares) and the JKW energy principle (circles). The dashed curve (diamonds) corresponds to the JKW solution for a bi-Maxwellian distribution function model.

toroidal Alfvén frequency $\omega_{At} = B_0 / \sqrt{\mu_0 \rho_M R_0^2}$. The growth rates as a function of $\langle \beta \rangle$ in Fig. 8 shows that the results with the slowing-down model (blue solid curve with circles) are very similar to those of the bi-Maxwellian (red dashed curve with diamonds) according to the JKW energy principle. The normalised growth rate peaks at $\omega/\omega_{At} = 0.1$ at $\langle \beta \rangle = 2\%$ and decreases by 60% when $\langle \beta \rangle$ reaches 4.5%. As a point of reference, we also plot the results of the slowing-down distribution function model with $\theta_b \sim 18°$ according to the KO energy principle (solid black curve with squares). The maximum growth rate from the KO model is $\omega/\omega_{At} = 0.3$ at $\langle \beta \rangle \sim 3\%$ and decreases by about 30% when $\langle \beta \rangle = 4.45\%$. The normalised growth rates as a function of $\langle \beta \rangle$ for injection angles of $\theta_b \sim 18°$, $\theta_b \sim 43.5°$, and $\theta_b \sim 68°$ are plotted in Fig. 9. The growth rates decrease slightly from parallel to perpendicular injection, but remain of the same order of magnitude and display the same trend as $\langle \beta \rangle$ is varied.

As a final application of the slowing-down distribution function model at $\theta_b \sim 18°$ with ANIMEC and TERPSICHORE, we investigate the fluid MHD stability according to

the JKW energy principle as a function of the peakedness of the hot particle pressure. For this study, we prescribe $p_h(s) = p_h(0)(1 - s)^k$ and vary $k$. For larger $k$, the hot particle contribution to the pressure becomes more peaked. We fix total $\langle \beta \rangle = 2.55\%$ and $\langle \beta_{th} \rangle = 1.7\%$. Marginal stability is achieved when $k > 4$ as illustrated in Fig. 10.

## VII. THE ELECTROSTATIC POTENTIAL

Future investigations of fast particle guiding centre orbits and energetic particle stability in the presence of unstable MHD fields require the identification of the electrostatic and electromagnetic potentials in terms of the perturbed MHD displacement vector components. Typically in guiding center codes, the perturbed vector potential is assumed to have only a finite component along the equilibrium magnetic field lines.[31] In our notation, this corresponds to $\delta A_\parallel = \sigma \Upsilon B$, where $\Upsilon$ represents the perturbed field amplitude. Evaluating the radial component of the perturbed MHD magnetic field $\delta \boldsymbol{B} \cdot \nabla s = \nabla \times (\boldsymbol{\xi} \times \boldsymbol{B})$, we can obtain a valid *albeit* nonunique relation between $\Upsilon$ and $\xi^s$. The invocation of Faraday's law relates the electrostatic potential $\Phi_E$ to $\Upsilon$, which then reads in Fourier space, as described in Ref. 32, as

$$\Phi_{Emn}(s) = -\frac{\omega}{\mu_0} \left[ \frac{\sigma \sqrt{g} B^2}{mI(s) - nJ(s)} \right] \xi_{mn}^s(s). \quad (13)$$

A more precise alternative is to consider the full $\delta \boldsymbol{A}$ model, thus including the $\delta B_\parallel$ terms that are neglected in the $\delta A_\parallel$ only reduced model.[32–34] This entails the application of the gauge transformation $\delta A_s = 0$,[32] from which we get

$$\Phi_{Emn}(s) = \omega \int_0^s ds \eta_{mn}(s). \quad (14)$$

In real space,

$$\Phi_E(s, \theta, \phi, t) = \sum_{mn} \Phi_{Emn}(s) \sin(m\theta - n\phi + \Delta - \omega t), \quad (15)$$

where $\Delta$ is a phase parameter.[30] The electrostatic potential of the $n = 2$ instability structure in LHD we have computed
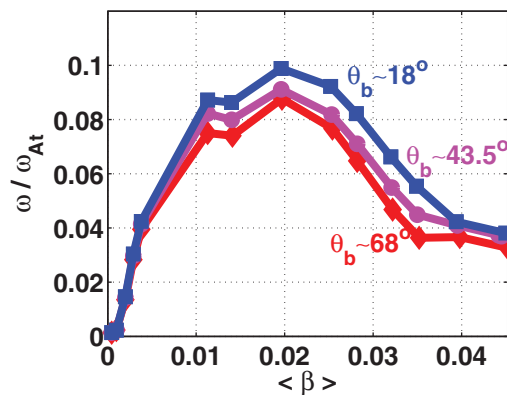


FIG. 9. Growth rate normalised to the toroidal Alfvén frequency for an inward-shifted LHD configuration as a function of $\langle \beta \rangle$ from a modified slowing-down distribution function with balanced beam injection angles of $\theta_b \sim 18°$ (squares), $\theta_b \sim 43.5°$, (circles) and $\theta_b \sim 68°$ (diamonds) with respect to the direction of the magnetic field lines according to the JKW energy principle.
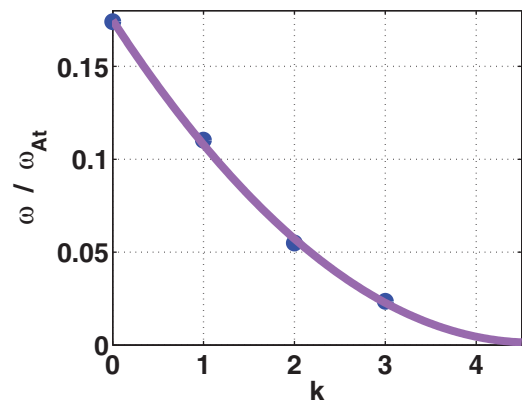


FIG. 10. Growth rate normalised to the toroidal Alfvén frequency for an inward-shifted LHD configuration as a function of the hot particle pressure peakedness factor $k$ at fixed $\langle \beta \rangle = 2.55\%$ from a modified slowing-down distribution function with balanced beam injection angle of $\theta_b \sim 18°$. The hot particle pressure factor is $p_h(s) = p_h(0)(1 - s)^k$.
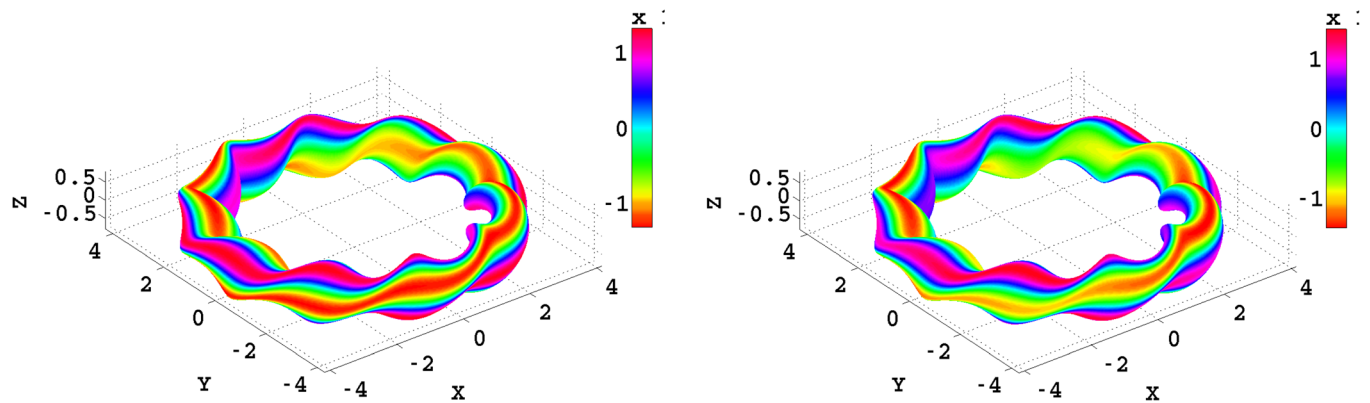
FIG. 11. The electrostatic potential $\Phi_e/\omega$ associated with an $n=2$ mode family fluid MHD instability calculated with the JKW model in LHD at $\langle \beta \rangle \simeq 4.45\%$ with fast particles injected at an angle of $\theta_b \sim 18°$ on a toroidal flux surface $\sqrt{s} \simeq 0.962$ near the edge of the plasma is plotted when only $\delta A_\parallel$ contributions are retained (left) and when the full electromagnetic field is computed (right).

with the JKW model at $\langle \beta \rangle \simeq 4.45\%$ demonstrates that retaining only finite $\delta A_\parallel$ effects may constitute an adequate approximation for $\Phi_E$ in guiding center computations. However, detailed numerical simulations will be necessary to verify this conjecture. Fig. 11 shows the toroidal structure of $\Phi_E$ on the flux surface for which $\sqrt{s} \simeq 0.962$. This reveals that the reduced model with finite $\delta A_\parallel$ only is slightly more extended toroidally compared to the full model which retains the finite $\delta B_\parallel$ contribution (the compressional Alfvén waves).

## VIII. SUMMARY AND CONCLUSIONS

The MHD equilibrium and fluid stability of a 10-field period inward-shifted heliotron configuration (vacuum magnetic axis $R_{ax} \sim 3.55$ m) that models the LHD device is investigated with the ANIMEC code and the TERPSICHORE code, respectively. A modified slowing-down distribution function has been adopted to generate anisotropic pressure equilibrium states in 3D geometry. This form is an alternative to a bi-Maxwellian distribution function studied extensively in the past that allows to model neutral beam injected ions with different angles of injection. The ANIMEC code has been extended to include this hot particle distribution function model for the computation of anisotropic pressure equilibrium states. We adjust the input parameters of the distribution function to obtain fixed boundary anisotropic equilibria with injection angles $\theta_b \sim 18°$ ($\langle p_\parallel^h \rangle > \langle p_\perp^h \rangle$), $\theta_b \sim 43.5°$ ($\langle p_\parallel^h \rangle \sim \langle p_\perp^h \rangle$), and $\theta_b \sim 68°$ ($\langle p_\parallel^h \rangle < \langle p_\perp^h \rangle$). Under zero toroidal current condition, the rotational transform is insensitive to injection angle up to $\langle \beta \rangle = 4.5\%$. The fast particle contribution to $\langle \beta \rangle$ in the calculations performed is 1/3, and the thermal pressure profiles applied are consistent with the experimental observation. The hot particle profiles are chosen to be more peaked than their thermal counterparts.

The linear fluid MHD stability with respect to the $n=2$ family of modes of the equilibrium states is determined with the TERPSICHORE code. We specifically concentrate on the rigid hot particle model proposed by JKW[24] because this model may reflect more accurately the experimental observations in the LHD heliotron device.[2] The kinetic energy mod-

ule in the TERPSICHORE code has been extended to investigate a more physical kinetic energy than has been previously considered. The stability studies as a function $\langle \beta \rangle$ indicate that for near tangential neutral beam injection ($\theta_b \sim 18°$), the slowing-down distribution function model yields very similar growth rates to that of the bi-Maxwellian model according to the predictions of the JKW energy principle approximation. The growth rate peaks at $\omega/\omega_{At} = 0.1$ when $\langle \beta \rangle \sim 2\%$ and decreases to below 0.04 at $\langle \beta \rangle \sim 4.5\%$. The fully interacting hot particle approach associated with the KO energy principle predicts growth rates peaking at $\langle \beta \rangle \sim 3\%$ at a growth rate $\omega/\omega_{At} = 0.3$, which decreases somewhat for higher $\langle \beta \rangle$. A comparative study of the linear growth rates of the $n=2$ family of MHD instability as a function of $\langle \beta \rangle$ shows a similar trend that is only weakly dependent on beam injection angle, with the more nearly parallel injection of $\theta_b \sim 18°$ being slighly more unstable than that at $\theta_b \sim 43.5°$, while the more perpendicular injection of $\theta_b \sim 68°$ is the least unstable. But the differences are small. Finally, a variation of the radial width of the fast particle pressure profile demonstrates that the plasma becomes MHD stable at $\langle \beta \rangle = 2.55\%$ according to the JKW energy principle when the profile is sufficiently peaked.

The electrostatic potential associated with the $n=2$ instability family at $\langle \beta \rangle \simeq 4.45\%$ we compute remains weakly sensitive to finite compressional Alfvén wave $\delta B_\parallel$ contributions.

Previously, we have developed and applied a linear gyrokinetic model to obtain a diamagnetic- drift-corrected balooning mode equation in the limit that the mode frequency is much smaller than the energetic particle drift frequency.[35,36] As a result, the hot particle pressure gradients do not contribute to the instability drive. In the JKW model we have considered, the fast particle current density and pressure gradients contribute neither to the mode stabilization nor its destabilization. This yields a subtle but small difference in the structure of the equations.[20]

Future research will concentrate on detailed comparisons of the fluid MHD stability with experimental observations and measurements. Drift kinetic theory simulations are expected to provide detailed information on the kinetic modifications of the fluid stability properties that we have computed with TERPSICHORE.

## ACKNOWLEDGMENTS

We are indebted to Dr. S. P. Hirshman for his invaluable contributions in the development of the ANIMEC code. An important fraction of the work described in this article was undertaken while WAC was a Guest Professor at the National Institute for Fusion Science. He thanks Professor A. Komori and Professor H. Yamada for their hospitality. This research was partially sponsored by the Fonds National Suisse de la Recherche Scientifique and Euratom.

[1] O. Motojima, N. Ohyabu, A. Komori *et al.*, Nucl. Fusion **43**, 1674 (2003).

[2] K. Y. Watanabe, S. Sakakibara, Y. Narushima, H. Funaba, K. Narihara, K. Tanaka, T. Yamaguchi, K. Toi, S. Ohdachi, O. Kaneko, H. Yamada, Y. Suzuki, W. A. Cooper, S. Murakami, N. Nakajima, I. Yamada, K. Kawahata, T. Tokuzawa, A. Komori, and LHD experimental group, Nucl. Fusion **45**, 1247 (2005).

[3] T. Yamaguchi, K. Y. Watanabe, S. Sakakibara, Y. Narushima, K. Narihara, T. Tokuzawa, K. Tanaka, I. Yamada, M. Osakabe, H. Yamada, K. Kawahata, K. Yamazaki, and LHD experimental group, Nucl. Fusion **45**, L33 (2005).

[4] W. A. Cooper, G. Bateman, D. B. Nelson, and T. Kammash, Nucl. Fusion **20**, 985 (1980).

[5] E. Salberta, R. C. Grimm, J. L. Johnson, J. Manickam, and W. M. Tang, Phys. Fluids **30**, 2796 (1987).

[6] T. Takeda and S. Tokuda, J. Comput. Phys. **93**, 1 (1991).

[7] W. Zwingmann, L. G. Eriksson, and P. Stubberfield, Plasma Phys. Controlled Fusion **43**, 1441 (2001).

[8] W. A. Cooper, S. P. Hirshman, and M. C. Depassier, Phys. Fluids **30**, 3532 (1987).

[9] H. Grad, Phys. Fluids **9**, 498 (1966).

[10] V. D. Pustovitov, Plasma Phys. Controlled. Fusion **52**, 065001 (2010).

[11] S. P. Hirshman and O. Betancourt, J. Comput. Phys. **96**, 99 (1991).

[12] S. P. Hirshman and J. C. Whitson, Phys. Fluids **26**, 3553 (1983).

[13] S. P. Hirshman, W. I. van Rij, and P. Merkel, Comput. Phys. Commun. **43**, 143 (1986).

[14] W. A. Cooper, S. P. Hirshman, R. Gruber, and S. Merazzi, Comput. Phys. Commun. **72**, 1 (1992).

[15] W. A. Cooper, S. P. Hirshman, T. Yamaguchi, Y. Narushima, S. Okamura, S. Sakakibara, C. Suzuki, K. Y. Watanabe, H. Yamada, and K. Yamazaki, Plasma Phys. Controlled. Fusion **47**, 561 (2005).

[16] W. A. Cooper, J. P. Graves, S. P. Hirshman, T. Yamaguchi, Y. Narushima, S. Okamura, S. Sakakibara, C. Suzuki, K. Y. Watanabe, H. Yamada, and K. Yamazaki, Nucl. Fusion **46**, 683 (2006).

[17] W. A. Cooper, S. P. Hirshman, P. Merkel, J. P. Graves, J. Kisslinger, H. F. G. Wobig, Y. Narushima, S. Okamura, and K. Y. Watanabe, Comput. Phys. Commun. **180**, 1524 (2009).

[18] C. Nührenberg, Phys. Plasmas **3**, 2401 (1996).

[19] D. V. Anderson, W. A. Cooper, R. Gruber, S. Merazzi, and U. Schwenn, Int. J. Supercomput. Appl. **4**, 34 (1990).

[20] W. A. Cooper, J. P. Graves, T. M. Tran, R. Gruber, Y. Narushima, S. Okamura, S. Sakakibara, C. Suzuki, K. Y. Watanabe, H. Yamada, and K. Yamazaki, Fusion Sci. Technol. **50**, 245 (2006).

[21] W. A. Cooper, J. P. Graves, M. Jucker, K. Y. Watanabe, Y. Narushima, and T. Yamaguchi, Plasma Phys. Controlled Fusion **49**, 1177 (2007).

[22] B. F. McMillan and R. G. Storer, J. Plasma Phys. **72**, 829 (2006).

[23] M. D. Kruskal and C. R. Oberman, Phys. Fluids **1**, 275 (1958).

[24] J. L. Johnson, R. M. Kulsrud, and K. E. Weimer, Plasma Phys. **11**, 463 (1969).

[25] J. G. Cordey and M. J. Houghton, Nucl. Fusion **13**, 215 (1973).

[26] Y. Nakamura, T. Matsumoto, M. Wakatani, S. A. Galkin. V. V. Drozdov, A. A. Martynov, Yu. Yu. Poshekhnonov, K. Ichiguchi, L. García, B. A. Carreras, C. Nührenberg (née Schwab), W. A. Cooper, and J. L. Johnson, J. Comput. Phys. **128**, 43 (1996).

[27] W. A. Cooper, G. Y. Fu, R. Gruber, S. Merazzi, U. Schwenn, and D. V. Anderson, in *Proc. Varenna-Lausanne Int. Workshop on Theory of Fusion Plasmas* (Editrice Compositori, Bologna, 1990), p. 655.

[28] C. Nührenberg (née Schwab), Phys. Fluids B **5**, 3195 (1993).

[29] A. Ardelea and W. A. Cooper, Phys. Plasmas **4**, 3482 (1997).

[30] W. A. Cooper, Plasma Phys. Controlled. Fusion **34**, 1011 (1992).

[31] R. B. White and M. S. Chance, Phys. Fluids **27**, 2455 (1984).

[32] W. A. Cooper, J. P. Graves, S. Brunner, and M. Yu. Isaev, Plasma Phys. Controlled. Fusion **53**, 24001 (2011).

[33] R. B. White, Phys. Fluids B **2**, 845 (1990).

[34] S. D. Pinches, L. C. Appel, J. Candy, S. E. Sharapov, H. L. Berk, D. Borba, B. N. Breizman, T. C. Hender, K. I. Hopcraft, G. T. A. Huysmans, and W. Kerner, Comput. Phys. Commun. **111**, 133 (1998).

[35] L. Brocher, W. A. Cooper, J. P. Graves, G. A. Cooper, Y. Narushima, and K. Y. Watanabe, Nucl. Fusion **50**, 025009 (2010).

[36] W. A. Cooper, L. Brocher, J. P. Graves, G. A. Cooper, Y. Narushima, and K. Y. Watanabe, Contrib. Plasma Phys. **50**, 713 (2010).